International Journal of Biological Macromolecules 357 (2026) 151666

Contents lists available at ScienceDirect

International Journal of Biological Macromolecules

journal homepage: www.elsevier.com/locate/ijbiomac

Intramolecular energy transfer to S-nitrosylated Cys residues is at the basis of fluorescence sensitivity to nitric oxide in the blue fluorescent protein mTagBFP2

Lucia Bellanova [a,1], Carlotta Viappiani [a,1], Antonio Scarano [b], Stefano Bruno [b], Keren Morreale [a,c], Arne Franzen [c], Beatrix Santiago-Schübel [d], Lorenzo Cupellini [e], Vera Svensson [f], Thomas Drepper [f], Stefania Abbruzzetti [a], Pietro Delcanale [a], Francesca Laneri [g], Salvatore Sortino [g], Armida Di Fenza [h], Riccardo Nifosì [h,*], Cristiano Viappiani [a,*], Thomas Gensch [c,*]

[a] Dipartimento di Scienze Matematiche, Fisiche e Informatiche, Università di Parma, Parma, Italy
[b] Dipartimento di Scienze degli Alimenti e del Farmaco, Università di Parma, Parma, Italy
[c] Institute of Biological Information Processing (IBI-1: Molecular and Cellular Physiology), Forschungszentrum Jülich, Jülich, Germany
[d] Institute of Biological Information Processing (IBI-7: Structural Biochemistry), Forschungszentrum Jülich, Jülich, Germany
[e] Dipartimento di Chimica e Chimica Industriale, Università di Pisa, Pisa, Italy
[f] Institute of Molecular Enzyme Technology, Faculty of Mathematics and Natural Sciences, Heinrich Heine University Düsseldorf, Forschungszentrum Jülich GmbH, Jülich, Germany
[g] Department of Drug and Health Sciences, University of Catania, Catania, Italy
[h] NEST, CNR-Istituto Nanoscienze and Scuola Normale Superiore, Pisa, Italy

A B S T R A C T

Fluorescent protein (FP) variants have recently emerged as promising intracellular nitric oxide (NO) sensors based on NO-induced fluorescence loss due to cysteine S-nitrosylation - the covalent addition of a nitroso group to a cysteine thiol within a protein to form an S-nitrosothiol. Here, we investigate the mechanisms underlying this fluorescence loss using a combined experimental and computational approach. We focus on mTagBFP2, a blue fluorescent protein that undergoes a 70% reduction in fluorescence quantum yield and lifetime upon exposure to micromolar NO concentrations. We discriminate, through mutagenesis, the contributions of two key cysteine residues and propose an unprecedented excitation energy transfer (EET) from the mTagBFP2 chromophore to the S-nitroso groups as a potential quenching mechanism. Our EET efficiency calculations incorporate full couplings, the effects of the surrounding protein and solvent, and molecular dynamics-based configurational flexibility. The computed EET efficiencies broadly align with experimental observations, with remaining discrepancies for which we advance potential explanations. Our findings establish a mechanistic basis for NO-induced fluorescence loss in mTagBFP2, providing guidelines for the rational design of next-generation NO-sensitive FPs. Moreover, they suggest that analogous S-nitrosylation–driven quenching mechanisms could be operative in other FPs with exposed cysteine residues, underscoring the risk of artefacts in cellular imaging under physiological NO levels.

1. Introduction

Nitric oxide (NO) is a small, diffusible free radical produced by nitric oxide synthases. NO is a critical cell signaling molecule that plays fundamental roles in both cell physiology and pathology. Understanding the NO dynamics in cells has always been considered fundamental to fully comprehend the underlying molecular mechanisms of NO action [1–5].

Despite the relevance of this messenger, only a limited number of methods are available to monitor intracellular NO, mostly because the development of suitable sensors has been impeded by the low concentration of the analyte, its short lifetime, and its reactivity.

In recent years, genetically encoded fluorescent sensors have been proposed to address this issue [6]. These molecular probes, generally multi-domain fusion proteins, have been designed to respond to changes in NO concentration through variations in their fluorescence emission properties, and allow for the direct or indirect visualization of NO formation and distribution in real time, with subcellular spatial resolution.

* Corresponding authors.
E-mail addresses: riccardo.nifosi@nano.cnr.it (R. Nifosì), cristiano.viappiani@unipr.it (C. Viappiani), t.gensch@fz-juelich.de (T. Gensch).
[1] These authors are co-first authors and contributed equally to this work.

https://doi.org/10.1016/j.ijbiomac.2026.151666
Received 19 October 2025; Received in revised form 17 March 2026; Accepted 24 March 2026
Available online 25 March 2026
0141-8130/© 2026 The Authors. Published by Elsevier B.V. This is an open access article under the CC BY license (http://creativecommons.org/licenses/by/4.0/).

For instance, the so-called geNOps probes consist of different FP variants fused to a bacteria-derived NO-binding domain. This domain, referred to as GAF, selectively binds NO via a non-heme iron (II) center. The NO-binding GAF domain brings the radical in close proximity to the chromophore of FPs, resulting in a rapid loss of fluorescence. The mechanism is fully reversible [7,8]. More recently, a different construct, termed GefiNO, was proposed as a ratiometric NO probe [9].

We recently reported a simple fluorescent structure, the blue fluorescent protein mTagBFP2 [10], able to sense NO through the changes induced in fluorescence emission intensity and lifetime [11]. Upon exposure to NO, emission intensity and lifetime undergo a parallel decrease, without any detectable spectral changes. Fig. 1 reports the absorption, fluorescence excitation, and fluorescence emission spectra for mTagBFP2 in PBS. The absorption spectrum (Fig. 1A, cyan solid curve) shows a distinct peak at 401 nm, which is coincident with the fluorescence excitation peak (Fig. 1A, blue dotted curve), whereas emission shows a peak at 454 nm (Fig. 1A, blue solid curve). Fig. 1B reports the fluorescence decay collected at 454 nm upon pulsed excitation at 380 nm. Analysis of the decay is obtained with a double-exponential function, yielding an average lifetime of 2.46 ns.

The small size of the protein (26.7 kDa), the lack of pH sensitivity of the absorption spectrum and of the fluorescence emission intensity and lifetime in the physiological range and further down to pH ~ 4, the improved photostability, the high extinction coefficient (50,600 ± 800 $M^{1-}cm^{-1}$), and the high fluorescence quantum yield (0.64), altogether contribute to an excellent performance of this reliable genetically encoded fluorescent probe [10].

Our previous studies demonstrated that the reduction in fluorescence yield and lifetime readily reports the presence of NO through S-nitrosylation of Cys residues of the protein [11]. While the decrease in fluorescence was found to correlate with S-nitrosylation of Cys residues in the amino acid sequence (Fig. 1C), the molecular determinants of the effect are yet to be understood. As described in the following, using a combination of experimental and theoretical studies, in this work we set out to determine the molecular origin of the fluorescence quenching observed upon S-nitrosylation of Cys residues in mTagBFP2. Steady-state and time-resolved fluorescence spectroscopy, and LC-MS on mTagBFP2 variants allow us to identify the residues responsible for the observed fluorescence quenching, confirming S-nitrosylation of specific Cys residues as the relevant process.

To assess the possible changes in local dynamics upon S-nitrosylation of Cys residues that may lead to excited state quenching of the chromophore, we simulate the molecular dynamics of mTagBFP2 with either non-modified or S-nitrosylated cysteine residues.

We then investigate the possibility of excitation energy transfer from the chromophore to the S-nitroso group(s) as a plausible mechanism of fluorescence quenching. We use a multiscale approach combining quantum chemistry methods for determining electronic couplings, with molecular mechanics methods to account for screening effects and to model the interplay between conformational motion and energy transfer efficiency. Such molecular-simulations-based approaches have reached a mature stage allowing for the reliable determination of energy transfer rates in biomolecular systems [12].

Finally, we discuss the implications of excitation energy transfer to the nitroso group in a wider context. We suggest that this hitherto neglected process needs to be considered for its possible interference in bioimaging applications involving cysteine-containing fluorescent proteins.

2. Results and discussion

2.1. Spectroscopic analysis of NO induced fluorescence loss in mTagBFP2 and its variants

The fluorescence response of mTagBFP2 upon exposure to NO generated by decomposition of MAHMA NONOate is summarized in Fig. 2. Steady-state fluorescence emission intensity (Fig. 2A) and time-resolved fluorescence emission (Fig. 2B) were collected as a function of time after NO was added to the solution (Supporting information Fig. S1A), which led to a reduction in both parameters. We estimated the extent of quenching from the asymptotic changes when equilibrium was reached, which occurred after ca. 1 h at room temperature. Fig. 2A-C also show that fluorescence quenching becomes stronger as NO concentration is increased, resulting in lower fluorescence emission intensity and average lifetime. By fitting the plots in Fig. 2C using a simple binding model, we conclude that the extent of maximum decrease is the same within experimental errors (68 ± 2% for ΔF/F and 65 ± 2% for Δτ/τ), with an apparent dissociation constant of 4.5 ± 0.3 μM for both fluorescence properties. The value of the apparent dissociation constant means that the sensor is suitable for detecting NO concentrations in the high-nM to μM range, as may be observed in macrophages in response to microbial infections [4,13]. or in vasodilation [14]. mTagBFP2 is not sensitive to NO dynamics in the pM to low-nM range, as encountered, e.g., in neurotransmission [3,15], and its utility is therefore restricted to those cases where NO is produced in sufficiently high concentration.

GSNO is a physiologically relevant NO donor. We determined the extent of fluorescence change upon S-nitrosylation of Cys residues by replicating the above experiments using GSNO as NO donor. As observed for the case of NO generated by MAHMA NONOate, the extent of fluorescence emission quenching progressively increases with GSNO concentration (Supporting Information Fig. S1D and E), although the overall time needed to complete the reaction is significantly longer

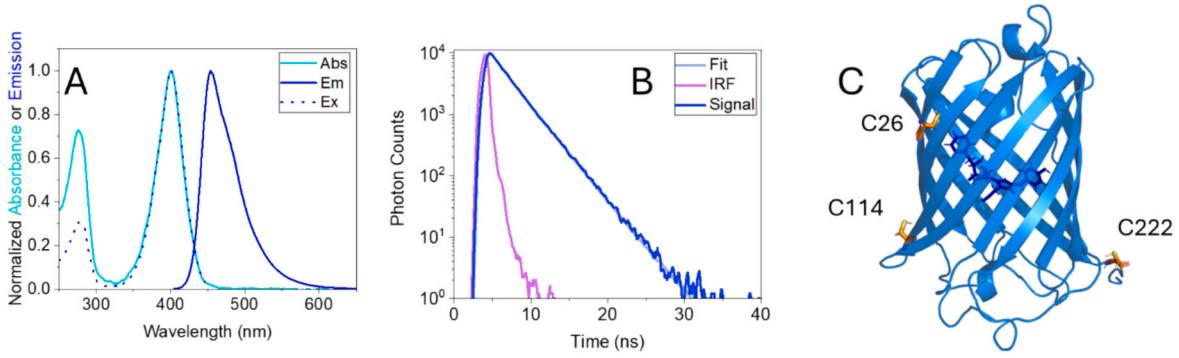


Fig. 1. Spectral properties of mTagBFP2 and its three-dimensional structure. A. Normalized absorption spectrum (solid cyan, λ_{max} = 401 nm), fluorescence excitation (dotted blue) and emission (solid blue, λ_{max} = 454 nm) spectra for a 0.4 μM solution of mTagBFP2 in PBS, pH = 7.4. The fluorescence excitation spectrum was collected through emission at 454 nm. Fluorescence emission was excited at 401 nm. B. Fluorescence decay for mTagBFP2. Excitation was at 380 nm, emission was collected at 454 nm. Average lifetime is 2.46 ± 0.05 ns (IRF = instrument response function). C. Cartoon representation of the modelled structure for mTagBFP2 (see Methods section in Supporting Information), where the Cys residues are drawn in yellow sticks and the chromophore in blue sticks.

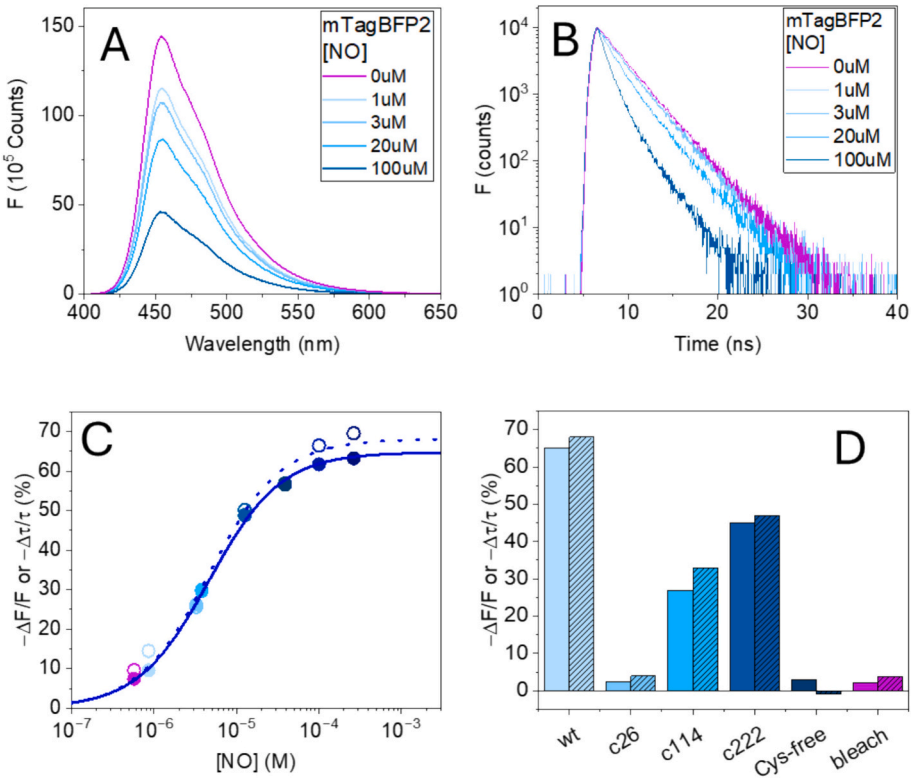


Fig. 2. Changes in fluorescence emission by mTagBFP2 in the presence of NO. A. Representative fluorescence emission spectra by mTagBFP2 at selected NO concentrations measured 1 h after addition of NO. The emission spectrum in the absence of NO is shown as the magenta curve. B. Representative fluorescence decays for mTagBFP2 at selected NO concentrations measured 1 h after addition of the concentrated NO solution. Excitation was at 380 nm, emission was detected at 454 nm. The fluorescence decay in the absence of NO is shown as the magenta curve. C. Percent change in Fluorescence intensity (open circles) and in average lifetime (filled circles) as a function of [NO]. The blue lines represent the best fits (solid for ΔF/F and dotted for Δτ/τ) to a simple binding model ($A + B \rightleftarrows AB$, where A = mTagBFP2 and B = NO). D. Percent change in fluorescence intensity (hatched bars) and in average lifetime (bars) for mTagBFP2 (wt), the single-Cys-containing variants (c26, c114, c222), and the Cys-free triple variant (C26A C114S C222S). The histogram also shows the extent of bleaching observed during the experiment for mTagBFP2 in the absence of NO.

(Fig. S1B), an indication that the reaction with GSNO has a higher free energy barrier to cross. While the corresponding plots for ΔF/F and Δτ/τ (Supporting Information Fig. S1F) are quite similar to those in Fig. 2C, the apparent dissociation constant has a slightly lower value. For the S-nitrosylation reaction induced by GSNO, we estimate a maximum drop in fluorescence intensity of 61 ± 2% with $K_d = 1.0 \pm 0.2$ μM. Fitting of Δτ/τ afforded similar values (58 ± 2%), with a slightly higher dissociation constant $K_d = 1.5 \pm 0.2$ μM. We emphasize that the overall change in fluorescence emission intensity and lifetime observed at saturating NO concentrations is remarkably large. However, we note that the full dynamic range in response to exposure of NO donors (Figs. 2C and S1F) refers to equilibrium conditions, that are attained after at least 30 min. Nevertheless, while the response time of the sensor to NO concentration changes is admittedly slow, it should be emphasized that a sizeable signal is observed already after a few seconds of exposure to NO (a ~ 10% change in fluorescence emission intensity and lifetime is observed for mTagBFP2 after 10 s of exposure to 100 μM NO, Fig. S1A-C). We note that the reactivity and the observed rate of S-nitrosylation reactions are remarkably sensitive to the environment where the Cys residue is found, and may become much faster in special cases [16–18].

To identify the Cys residues subject to S-nitrosylation, we generated single-Cys-containing variants. In the developed mutants, the solvent-exposed C114 and C222 were replaced through conservative mutations by polar Ser residues, whereas C26, pointing to the interior of the barrel, was substituted by the more hydrophobic Ala. These variants do not show significant changes in absorption and fluorescence emission spectra (Supporting Information, Fig. S2), and only minor changes in fluorescence lifetime and quantum yield (Supporting Information, Table S1). We exposed each variant to a saturating GSNO concentration (100 μM). After reaching equilibrium, we determined the overall changes in fluorescence emission intensity and lifetime.

Fig. 2D compares the change in fluorescence emission intensity and lifetime for wt mTagBFP2 and the variants C114S C222S (c26), C26A C222S (c114), and C26A C114S (c222) after exposure to 100 μM GSNO. For comparison we also show the signal measured for the variant C26A C114S C222S (Cys-free), and the signal observed for wt mTagBFP2 in the absence of GSNO. Representative kinetics are shown in Fig. S1C. The fluorescence of variants containing Cys114 or Cys222 was found to be quite sensitive to NO. On the other hand, exposure of c26 variant to 100 μM GSNO results in barely detectable changes in fluorescence intensity and lifetime. The observed change is comparable to that shown by the Cys-free variant, suggesting that Cys26 is not reactive, possibly because of its topological position in the mTagBFP2 barrel (see Fig. 1C). Analogous experiments on c26 with the donor MAHMA NONOate afforded similar results (i.e. no change in fluorescence emission was observed, data not shown). Importantly, the small change observed for Cys-free and c26 variants is almost identical to the change observed for wt mTagBFP2 in the absence of NO, a change which can be interpreted as a result of minor bleaching of the mTagBFP2 chromophore during collection of experimental data. This leads us to conclude that NO has negligible effects on the fluorescence emission in Cys-free and c26 variants, in keeping with the idea that NO does not bind to the protein, either because there are no Cys residues (Cys-free) or because the Cys is not reactive (c26).

We note that the quenching of fluorescence in response to exposure to NO was observed also in cellular environment. Wide-field images

collected on mTagBFP2-overexpressing *E. coli* (Fig. 3A, transmitted; Fig. 3B, wide-field) revealed mTagBFP2 present throughout the bacteria, where some cells had higher mTagBFP2 accumulation at the cell pole(s). Fluorescence lifetime of intracellular mTagBFP2 was obtained by time-correlated single-photon counting (TCSPC) analysis of photon bursts in Fluorescence Correlation Spectroscopy experiments. Fig. 3C reports a representative photon burst for which the TCSPC analysis afforded the fluorescence decay reported in Fig. 3D (magenta trace). Exposure of bacteria to NO released from MAHMA NONOate (1 mM) resulted in a detectable decrease in lifetime ($\Delta\tau/\tau \sim$ -13%). Based on the calibration plot in Fig. 2C, we estimate that the effective average NO concentration inside bacteria was about 1.3 μM at equilibrium with 1 mM NO in extracellular solution. The smaller change in fluorescence lifetime observed in bacteria can be rationalized by considering that the reducing power of the cellular environment, with reported values of the cytoplasmic redox potential in *E. coli* ranging between −260 and − 280 mV [19] [20], will decrease the amount of nitrosylated Cys residues, even in the presence of mM NO concentration in the buffer solution where cells are immersed.

2.2. Mass Spectrometry (LC-MS) of mTagBFP2 and its Variants

To support the interpretation of the findings of the fluorescence spectroscopy measurements, LC-MS was applied to wt mTagBFP2, the Cys-free and the single-Cys-containing variants, respectively. The mass of the proteins was determined before (MW_{meas} without GSNO) and after (MW_{meas} with GSNO) a 2-h exposure to GSNO (saturating concentration 100 μM) (Table 1). The expected value, MW_{theor}, based on the amino acid sequence, is reported for comparison. While for mTagBFP2 the mass difference corresponds to the addition of two nitroso groups, as reported in our previous work [11], the Cys-free variant and the single Cys variant c26 showed no mass difference. Consistently, single Cys variants c114 and c222 both showed a mass increase corresponding to one added NO molecule upon S-nitrosylation in the presence of GSNO.

Table 1
Protein masses determined for different mTagBFP2 variants with and without exposure to GSNO.

mTagBFP2 variant	MW_{theor} (Da)	MW_{meas} (Da) without GSNO	MW_{meas} (Da) with GSNO	Mass difference (Da)
WT	27,479	27,480	27,538	+ 58
Cys-free (C26A C114S C222S)	27,416	27,415	27,415	0
c222 (C26A C114S)	27,432	27,431	27,460	+ 29
c114 (C26A C222S)	27,432	27,431	27,460	+ 29
c26 (C114S C222S)	27,448	27,447	27,447	0

2.3. Modelling the fluorescence quenching by S-nitrosylated Cys

The results shown above demonstrate that Cys S-nitrosylation of Cys114 and Cys222 leads to a decrease in fluorescence lifetime, a clear indication that the interaction leading to fluorescence quenching is dynamic in nature and occurs between the excited state of the

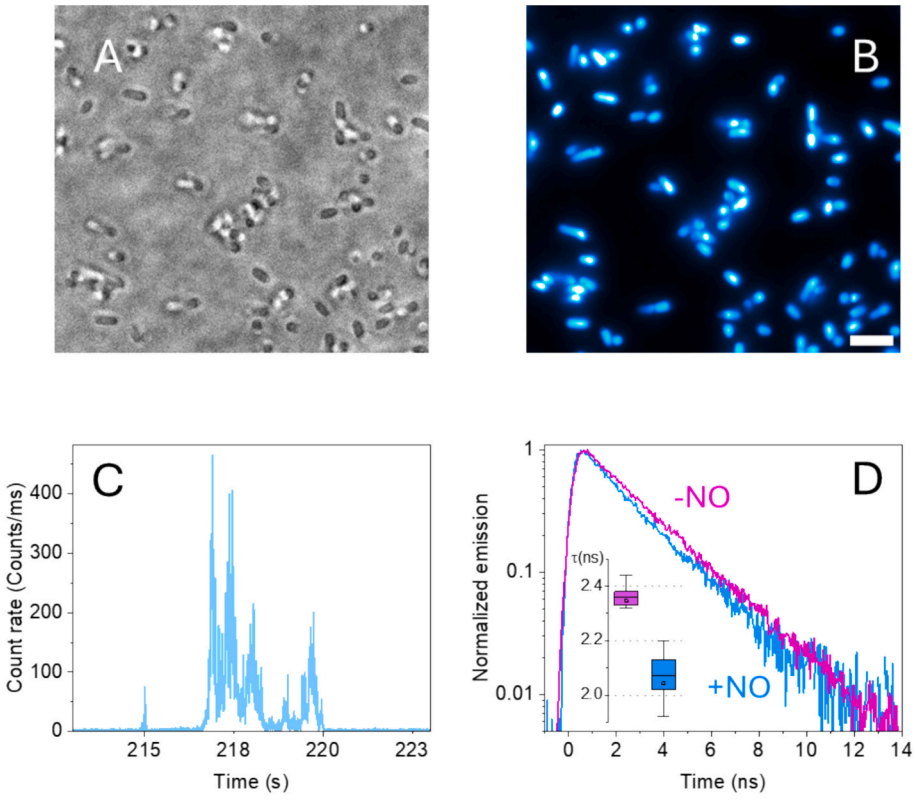


Fig. 3. Changes in fluorescence lifetime in *E. coli* (BL21(DE3)) expressing mTagBFP2 upon exposure to NO. A. Bright-field image of *E. coli* (BL21(DE3)) expressing mTagBFP2. Wells were pre-treated with poly-L-lysine to immobilize bacteria. B. Corresponding wide-field image of *E. coli* expressing mTagBFP2. Scale bar = 5 μm. Excitation wavelength = 405 nm. C. Representative time trace (1 ms binning) for the fluorescence emission collected with a confocal microscope for a suspension of mTagBFP2 expressing *E. coli* (BL21(DE3)) cells showing fluorescence bursts connected to single bacteria passing the confocal volume. Excitation at 405 nm, emission at 438/25 nm. From the analysis of the cross-correlation curves, we retrieved a diffusion coefficient D = 0.35 $\mu m^2/s$ (τ_D = 63 ms), consistent with diffusion of freely floating *E. coli* cells. D. Fluorescence decays retrieved from the bursts (a representative burst is shown in panel C), collected for an mTagBFP2-expressing *E. coli* suspension in the absence (magenta, average lifetime 2.35 ± 0.06 ns, 19 bursts) and in the presence of 1 mM NO (blue, average lifetime 2.04 ± 0.13 ns, 10 bursts). Inset to panel D reports a box plot for the lifetimes associated with the analyzed bursts, in the absence and in the presence of NO.

mTagBFP2 chromophore and the protein scaffold with S-nitrosylated Cys residues [21]. We therefore explore possible dynamic couplings between the chromophore excited state and S-nitrosylated Cys residues. Having identified a correlation between the observed fluorescence quenching and S-nitrosylation of Cys114 and Cys222, it remains to understand the physical mechanism underlying the quenching. As described below, our approach considers two different types of dynamic coupling: i) influence of S-nitrosylation on mTagBFP2 protein structure and dynamics; ii) excitation energy transfer from mTagBFP2 chromophore to S-nitrosylated Cys residues.

2.3.1. *Influence of S-nitrosylation on mTagBFP2 protein structure and dynamics*

S-nitrosylation may lead to changes in protein dynamics around the chromophore, which could potentially perturb the excited state, as hypothesized in our previous work [11]. We performed molecular dynamics (MD) simulations on the μs timescale of mTagBFP2 with S-nitrosylated Cys (CysNO) at positions 114 and 222. For comparison, we also simulated the unmodified, i.e. not nitrosylated, case. Our simulations uncover no significant change in structure or dynamics in the β-barrel and/or in the chromophore environment, as revealed by the root mean square deviation (RMSD) between the MD average structures, and the root mean square fluctuations (RMSF) of the β-barrel and of the chromophore in particular (Fig. S3). The two Cys residues are in both cases solvent-exposed and in rather peripheral positions, and in particular 222 is located at the beginning of the flexible C-terminus. They do not seem to engage in stable interactions with any of the surrounding residues, both in the unmodified and S-nitrosylated case, though nitrosylation has some effects on the gyration radius of the C-terminus, which becomes slightly more extended (Fig. S4). Thus, no conclusive evidence could be found supporting a role for protein dynamics in the quenching of the excited state upon Cys S-nitrosylation. Consequently, alternative processes have to be considered.

2.3.2. *Excitations of the S-nitroso group, spectral overlap and Förster radius*

A possible source of interaction between the excited state of the mTagBFP2 chromophore and the environment may arise from the formation of the chromophoric group SNO upon Cys S-nitrosylation. The spectral overlap between mTagBFP2 fluorescence and S-nitroso group absorption in GSNO (Fig. 4) suggests the possibility of excitation energy transfer (EET, also known as resonance energy transfer or electronic energy transfer) from the chromophore to the CysNO upon excitation of the fluorescent protein. Indeed, GSNO contains the S-nitrosylated Cys side chain (C-CH_2-SNO) and can therefore serve as a model for the absorption of the CysNO. Determining the efficiency of this EET for each nitrosylated Cys is essential to establish its potential contribution to the observed mTagBFP2 quenching. The efficiency of a relaxation channel c, defined as the ratio of its rate to the sum of all possible concurrent decay rates, i.e. $E = k_c / \sum k$, is in turn equal, in absolute value, to the ensuing relative variation of fluorescence $\Delta F/F$ and lifetime $\Delta\tau/\tau$.

From the spectral overlap integral and taking into account the chromophore-CysNO distances it is straightforward to give a first estimate of EET efficiency using Förster theory [22,23] (E^F_{EET}), whereby

$$E^F_{EET} = \frac{R_0^6}{R^6 + R_0^6} \quad (1)$$

Here R is the distance between donor and acceptor, and R_0 is the Förster radius, which depends on the overlap integral of the donor emission and acceptor absorption spectra and on the orientation of donor and acceptor transition dipole moments (TDM). Considering a random orientation of the TDMs (see methods section in the SI), we get values of R_0 of 1.40 nm or 1.29 nm depending on whether the refractive index of water ($n = 1.33$) or a more appropriate one for the inside of proteins ($n = 1.5$) is used (see discussion in ref. [24]) (Table 2).

This preliminary estimation of EET efficiency shows that it can give a non-vanishing contribution to the observed fluorescence quenching. However, while the efficiency is similar to the experimental value of $\Delta F/F$ for CysNO 114, the estimate is much lower than the observed values in the case of the c222 variant (the one containing a single Cys at 222). We note that, though in our simulations both Cys residues are present, their effects can be treated independently, as they are spatially rather separated and do not influence each other.

A more precise description of EET requires an in-depth analysis of the structural and electronic properties of the S-nitrosylated Cys side chain. Due to the interplay between various resonance structures, the S-nitroso

Table 2
EET efficiency estimated according to Förster theory assuming $\kappa^2 = 0.66$.

	R[a] (nm)	E^F_{EET}(%) $n = 1.33$	E^F_{EET} (%) $n = 1.5$	Exp
CysNO 114	1.6	31	21	27–32
CysNO 222	2.3	5	3	45–47

[a] Average values from the MD simulations, taking the centers of the π-conjugated systems

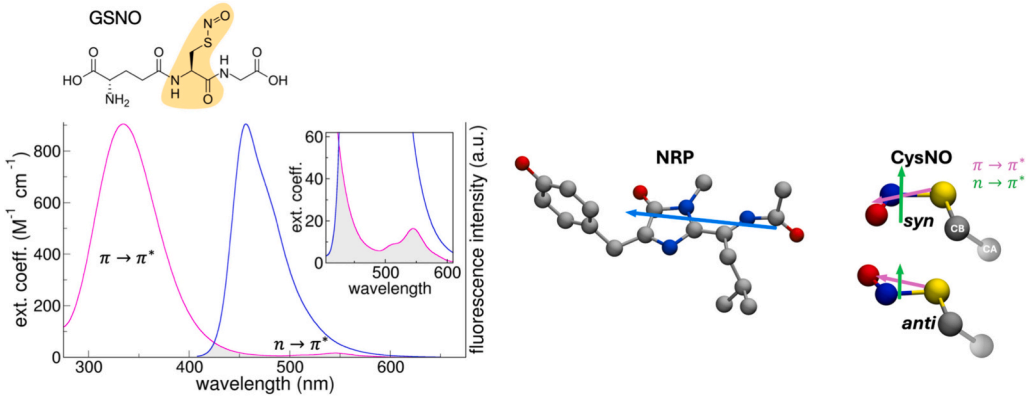


Fig. 4. Overlap between mTagBFP2 fluorescence emission and S-nitrosylated Cys absorption spectra. Left. Absorption spectrum of GSNO (magenta curve) and emission spectrum of mTagBFP2 (blue curve). The inset shows a zoom of the $n \rightarrow \pi^*$ band. GSNO structure is reported at the top, and the shaded area corresponds to the whole S-nitrosylated Cys (CysNO). The shaded area corresponds to the overlap between the two spectra (see also Fig. S5 in the supporting information). The structure of the mTagBFP2 chromophore (NRP) and of CysNO in the two *syn* and *anti* conformations are shown on the right, together with the transition dipole moments (colored arrows) of the relevant electronic transitions. With respect to NRP, the transition dipole moments for CysNO $\pi \rightarrow \pi^*$ and $n \rightarrow \pi^*$ are scaled up by a factor of 3 and 30 respectively (the calculated values are reported in the supporting information Tables S3 and S4). Atoms are colored according to the usual convention, with carbon atoms in grey, oxygen in red, nitrogen in blue and sulphur in yellow.

group exhibits a complex chemistry, in terms of structure, stability and reactivity [25]. The SN bond has a partial double-bond character, which separates the two *syn* and *anti* (or *cis* and *trans*) isomers. Several experimental [26,27] and theoretical [27–30] studies point to a higher stability of the *syn* configuration in primary S-nitrosothiols, such as GSNO and CysNO. Furthermore, the two bands in the GSNO absorption spectrum (Fig. 4) arise from two distinct excitations of the S-nitroso group, a weak $n\rightarrow\pi^*$ transition (peaking at 545 nm with $\varepsilon = 16.3\ M^{-1}\ cm^{-1}$) and a stronger $\pi\rightarrow\pi^*$ transition (peaking at 335 nm with $\varepsilon = 904.8\ M^{-1}\ cm^{-1}$). High-level quantum chemistry studies of methyl-thionitrite (CH_3SNO) [29] confirm this assignment and also show that the two configurations, *syn* and *anti,* have slightly different excitation energies and strengths, the *syn* configuration having both excitations blue-shifted by 1000–1500 cm^{-1} and with enhanced dipole strengths (by a factor of 1.5–2). Hence, two EET channels ($n\pi^*$ and $\pi\pi^*$) exist for each CysNO acceptor, each modulated by the *syn/anti* configuration.

2.3.3. *Efficiency of excitation energy transfer from molecular simulations*

We summarize in Table 3 the results of two different approaches to calculate EET rates and efficiencies, applied to the configurations from MD simulations. Both methods and in-depth analysis of the results are detailed in the SI (Section S3). The first method is the classic Förster theory averaged over the conformations from the MD trajectory, by taking into account the instantaneous donor-acceptor distances and TDM orientations for each of the two transitions. The second method, TrEsp–MMPol [12,31,32], evaluates the full Coulomb coupling of donor and acceptor electronic transition densities, approximated with suitably placed "transition charges". The contribution of the surrounding medium is modelled by polarizable dipoles responding to these transition densities. With respect to Förster theory, TrEsp-MMPol accounts for terms beyond the dipole-dipole approximation and can be applied in the case of anisotropic media such as that in the present case, where the donor is located inside the protein and the CysNO acceptor(s) are partially or completely solvent-exposed. In Förster theory these effects are accounted for by the refractive index, the choice of which is not obvious in the present case, as mentioned above.

The two methods lead to similar average EET efficiencies. Förster theory, however, significantly underestimates the EET rate in the case of the $n\rightarrow\pi^*$ transition, in particular for CysNO 222. The two approaches also yield different distributions of EET efficiencies during the MD trajectory, as apparent from Fig. 5. Notably, for CysNO 222, the high-E_{EET} tails extend to larger values in TrEsp-MMPol (up to 45% vs 30% in Förster theory).

Thanks to the biased-exchange simulations, both the *syn* and *anti* configurations of CysNO are sampled during the MD trajectories, and the averages within each subpopulation are reported in Table 3. The *syn* conformer generally exhibits higher EET rates, in part due to its larger dipole strength. We observe that the lower population of *syn* vs *anti* in

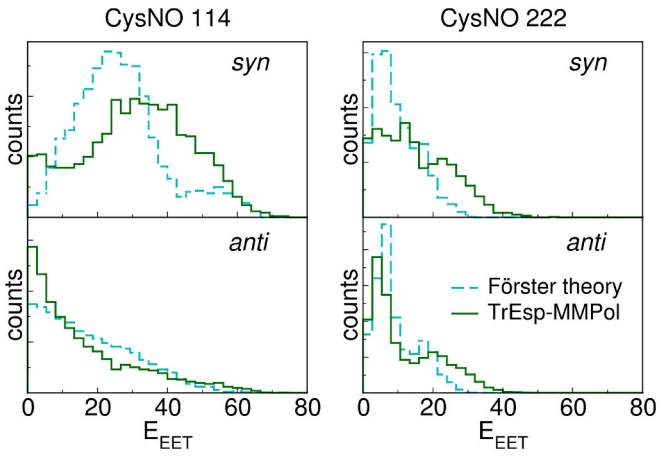


Fig. 5. Distribution of E_{EET} values calculated with Förster theory and TrEsp-MMPol during the simulation. A total of 5000 evenly spaced snapshots were analyzed.

our simulations is not an effect of interactions with the rest of the protein, as this trend also holds for the isolated CysNO (Fig. S11). This partitioning is inconsistent with the already discussed higher stability of the *syn* isomer in primary S-nitrosothiol [27,28], highlighting a potential limitation of the force field for CysNO [33]. To account for this deviation, we also provide in Table 3 reweighed energy transfer estimates ($\langle E_{EET}^{rew}\rangle$) based on a *syn/anti* ratio of 65/35. Using this adjusted population model and the more accurate TrEsp-MMPol approach, the resulting values increase to 26% for CysNO 114, 14% for CysNO 222, and 34% for their combined effect. According to the rule of combination (see note in Table 3), using the experimental values for the c114 and c222 variants yields a combined efficiency (and thus $-\Delta F/F$) of 54–58%, which is broadly consistent with the 65–68% measured for wt mTagBFP2.

In comparison to the experimental results, the result for CysNO at position 114 aligns well with the quenching observed in the c114 variant with a single Cys at 114 (30%), while the value for CysNO at position 222 accounts for only a portion of the quenching measured experimentally (40–45%). There are, however, potential shortfalls in our calculations that may explain this discrepancy. The GSNO absorption spectrum, which we used to calculate the overlap integrals, may not accurately represent the case of CysNO side chains of the protein, which, though solvent-exposed, may still engage in interactions with surrounding residues (among which Arg220 and Asp223 in the case of CysNO 222). Interactions with charged and polar residues were shown to strongly modify the electronic structure of the S-nitroso group [25], potentially leading to shifts in excitation energies and strength. We

Table 3
EET efficiencies and rates calculated using various approaches

CysNO	pop	$\langle k_{EET}^{n\pi}\rangle$	$\langle k_{EET}^{\pi\pi}\rangle$	$\langle E_{EET}^{F}\rangle$	$\langle E_{EET}^{F\ rew}\rangle$[a]	$\langle k_{EET}^{n\pi}\rangle$	$\langle k_{EET}^{\pi\pi}\rangle$	$\langle E_{EET}\rangle$	$\langle E_{EET}^{rew}\rangle$[a]
	(%)	($s^{-1} \times 10^6$)		(%)	(%)	($s^{-1} \times 10^6$)		(%)	(%)
		Förster Theory (n = 1.33[c])				TrEsp-MMPol			
114		46	77	20	24	77	55	21	26
anti	71	48	57	18		53	47	16	
syn	29	43	126	26		136	74	30	
222		9	36	10	10	31	35	13	14
anti	70	9	36	9		30	31	12	
syn	30	8	38	10		34	43	15	
114+222[b]				27	32			29	34

[a] Re-evaluated using a 65/35 *syn/anti* population ratio. See main text

[b] For two uncoupled acceptors $E_{EET}^{A1+A2} = \left(E_{EET}^{A1} + E_{EET}^{A2} - 2E_{EET}^{A1}E_{EET}^{A2}\right)/\left(1 - E_{EET}^{A1}E_{EET}^{A2}\right)$

[c] We should note that the use of water refractive index is not fully justified. However, using the more protein-like $n = 1.5$ leads to lower efficiencies of 13% and 6% for CysNO 114 and CysNO 222, respectively, resulting in a total energy transfer efficiency of 18%.

examined the sensitivity of our predictions to excitation energy shifts (SI, Section S3.7) and showed that moderate shifts of ~1000 cm^{-1} can lead to sizable variation of the estimated EET efficiencies (reaching values up to 25–30% in the case of CysNO 222). A related issue is the presence of potential inaccuracies in describing these interactions – especially due to the lack of explicit polarisation in the force field – and subsequent misrepresentation of the statistical weight of configurational subpopulations. One example is the already discussed *syn/anti* population ratio, but the argument might extend to configurations with high EET rate not being properly stabilised (see Fig. S13). Future work is needed to clarify these effects.

We cannot however exclude the presence of additional quenching mechanisms discriminating position 222 over 114. Past studies have shown that upon excitation in either of the two absorption bands the S-nitroso group can undergo *syn-anti* (*cis-trans*) photoisomerization around the S—N bond [34], and also photolysis [35,36], which results in the detachment of the NO• group. The release of NO• on the surface of the beta barrel may promote its entrance into the protein through transient channels (SI, Section S4) and eventual interaction with the chromophore, possibly leading to quenching of fluorescence through radical-induced non-radiative decay pathways.

2.4. A potentially general fluorescence quenching mechanism

The efficiency for EET between the mTagBFP2 chromophore and the nitrosylated Cys residues suggests that this mechanism may be operating also in other fluorescent proteins and thus have a wider significance. We have previously reported that fluorescence quenching is observed upon exposure of EGFP, EYFP, and TagRFP-T to nitric oxide [11].

Fig. 6D compares the experimental values derived from fluorescence quenching, with the estimate based on Förster theory, assuming $\kappa^2 = 0.66$ and $n = 1.33$. While these values would require a more accurate evaluation as proposed for mTagBFP2, it is nevertheless important to realize that fluorescence quenching occurs whenever these proteins are exposed to appreciable (i.e. μM) NO concentrations. This may result in unpredicted spurious signals when fluorescent proteins with exposed Cys are used within genetic constructs devised to sense different molecular species [37,38].

On the other hand, to the best of our knowledge, reaction of Cys residues with other relevant cellular metabolites does not lead to formation of groups with absorption in the visible-near UV [39], thus providing a selective physical observable for sensing Cys S-nitrosylation. A possible interference with Cys S-nitrosylation by NO may originate from reduced glutathione (GSH). GSH may bind to cysteinyl residues in proteins by creating reversible disulfide bonds, depending on the cysteine position and redox potential [40]. Given the relatively high cytosolic concentration of GSH (1–15 mM) [41], this may reduce the fraction of S-nitrosylated Cys residues in response to exposure to NO. However, the effects of S-nitrosylation of cytoplasmic mTagBFP2 expressed in mammalian cells [11] and in bacteria (Fig. 2) are clearly detectable in any case.

3. Conclusions

By a combined experimental and computational approach, we investigated the mechanisms of NO sensitivity of the fluorescent protein mTagBFP2, which is linked to the S-nitrosylation of two solvent-exposed Cys residues, one at position 114 and the other at 222. Controls on mTagBFP2 variants lacking these two Cys confirmed their role. We were able to separate the contributions of each Cys, by producing mTagBFP2

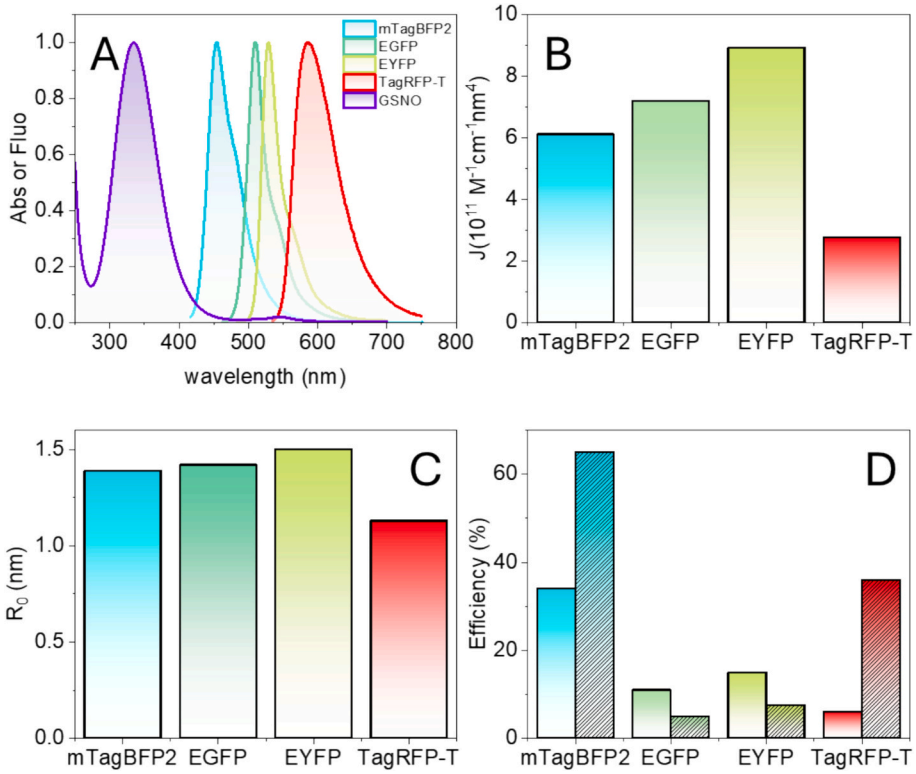


Fig. 6. FRET efficiencies for fluorescent proteins of different colors. A. Overlap between the normalized absorption spectrum of GSNO (purple curve) and the normalized emission spectra of mTagBFP2 (cyan curve), EGFP (green curve), EYFP (yellow curve), TagRFP-T (red curve). B. Overlap integrals between absorption spectrum of GSNO and mTagBFP2, EGFP, EYFP, and TagRFP-T. C. Förster radius for energy transfer between GSNO and mTagBFP2, EGFP, EYFP, and TagRFP-T. D. Comparison between calculated FRET efficiencies (solid bars) and experimentally determined fluorescence quenching (hatched bars) upon Cys S-nitrosylation. EET efficiency estimated according to Förster theory assuming $\kappa^2 = 0.66$ and $n = 1.33$. For EGFP and EYFP only Cys48 was considered, Cys70 is completely buried in the barrel and unlikely to react with NO. For TagRFP-T only Cys114 and Cys222 were considered. Cys172 is buried in the barrel and unlikely to react with NO.

variants containing only one of the two Cys. At saturating NO concentration, the fluorescence was quenched by 30% in the variant containing the single Cys114 and by 45% in Cys222, despite the latter being more distant from the chromophore. The quenching was accompanied by an analogous shortening of fluorescence lifetime. Given the overlap of mTagBFP2 emission spectrum with the absorption of the S-nitroso group, we speculated that intramolecular excitation/resonance energy transfer (EET) is contributing to the observed quenching. A careful estimation of EET efficiency by molecular simulations led to the conclusion that the quenching by CysNO 114 can be fully explained by the energy transfer process, whereas EET accounts only for part of the observed quenching in the case of Cys222, unless ad hoc hypotheses are formulated regarding the configuration of S-nitrosylated Cys222 and/or shifts in its excitation energies. Overall, our findings highlight the role of the EET mechanism in the NO sensitivity of fluorescent proteins. The reliable predictability of EET makes it particularly promising as a guiding principle for the rational design of novel FP-based NO biosensors with optimized efficiency. Studies in this direction are currently underway. The NO concentration range detectable by mTagBFP2 and other Cys containing fluorescent proteins is essentially determined by the chemistry supporting its reaction with Cys residues. As such, this class of NO sensors will share a similar concentration sensitivity range, although with different dynamic ranges depending on the topological position of the Cys residues and the spectral overlap between the fluorescent protein emission and the SNO absorption spectra. Our findings suggest that the same EET mechanism could be at play in other fluorescent proteins with solvent-exposed Cys residues and should be carefully factored into the design and calibration of genetically encoded fluorescent sensors. More broadly, EET to NO-bound species will need to be taken into account in future investigations of chromophoric systems that exhibit NO-induced fluorescence quenching, such as the GeNOps sensors.

CRediT authorship contribution statement

Lucia Bellanova: Visualization, Investigation, Formal analysis, Data curation. **Carlotta Viappiani:** Visualization, Investigation, Formal analysis, Data curation. **Antonio Scarano:** Resources, Investigation. **Stefano Bruno:** Resources, Investigation. **Keren Morreale:** Investigation. **Arne Franzen:** Resources. **Beatrix Santiago-Schübel:** Visualization, Investigation. **Lorenzo Cupellini:** Writing – review & editing, Software. **Vera Svensson:** Resources. **Thomas Drepper:** Writing – review & editing, Resources. **Stefania Abbruzzetti:** Writing – review & editing, Supervision, Conceptualization. **Pietro Delcanale:** Writing – review & editing, Visualization, Investigation. **Francesca Laneri:** Investigation. **Salvatore Sortino:** Writing – review & editing, Supervision, Project administration, Funding acquisition, Conceptualization. **Armida Di Fenza:** Writing – review & editing, Visualization, Formal analysis, Data curation. **Riccardo Nifosì:** Writing – review & editing, Writing – original draft, Supervision, Project administration, Funding acquisition, Formal analysis, Conceptualization. **Cristiano Viappiani:** Writing – review & editing, Writing – original draft, Supervision, Project administration, Funding acquisition, Conceptualization. **Thomas Gensch:** Writing – review & editing, Writing – original draft, Supervision, Resources, Project administration, Funding acquisition, Conceptualization.

Declaration of competing interest

The authors declare that they have no known competing financial interests or personal relationships that could have appeared to influence the work reported in this paper.

Data availability

Data will be made available on request.

Acknowledgements

This research was funded by the European Union – NextGenerationEU PNRR-M4C2- I1.1 – MUR Call for proposals n. 1409 del 14-09-2022 – Bando PRIN 2022 PNRR - ERC sector PE4-Project title: A molecular platform for intracellular nitric oxide sensing- Project Code P2022F4WR8- CUP Code D53D23016840001.

We acknowledge the CINECA award under the ISCRA initiative, for the availability of high-performance computing resources and support.

Appendix A. Supplementary data

Supplementary data to this article can be found online at https://doi.org/10.1016/j.ijbiomac.2026.151666.

References

[1] J.O. Lundberg, E. Weitzberg, Nitric oxide signaling in health and disease, Cell 185 (2022) 2853–2878, https://doi.org/10.1016/j.cell.2022.06.010.
[2] J. Tejero, S. Shiva, M.T. Gladwin, Sources of vascular nitric oxide and reactive oxygen species and their regulation, Physiol. Rev. 99 (2019) 311–379, https://doi.org/10.1152/physrev.00036.2017.
[3] S.M. Andrabi, N.S. Sharma, A. Karan, S.S. Shahriar, B. Cordon, B. Ma, J. Xie, Nitric oxide: physiological functions, delivery, and biomedical applications, Adv. Sci. 10 (2023) 2303259, https://doi.org/10.1002/advs.202303259.
[4] F.C. Fang, Antimicrobial reactive oxygen and nitrogen species: concepts and controversies, Nat. Rev. Microbiol. 2 (2004) 820–832, https://doi.org/10.1038/nrmicro1004.
[5] B.J. Mueller, M.D. Roberts, C.B. Mobley, R.L. Judd, A.N. Kavazis, Nitric oxide in exercise physiology: past and present perspectives, Front. Physiol. 15 (2025) 1504978, https://doi.org/10.3389/fphys.2024.1504978.
[6] E. Eroglu, S. Charoensin, H. Bischof, J. Ramadani, B. Gottschalk, M.R. Depaoli, M. Waldeck-Weiermair, W.F. Graier, R. Malli, Genetic biosensors for imaging nitric oxide in single cells, Free Radic. Biol. Med. 128 (2018) 50–58, https://doi.org/10.1016/j.freeradbiomed.2018.01.027.
[7] E. Eroglu, B. Gottschalk, S. Charoensin, S. Blass, H. Bischof, R. Rost, C.T. Madreiter-Sokolowski, B. Pelzmann, E. Bernhart, W. Sattler, et al., Development of novel FP-based probes for live-cell imaging of nitric oxide dynamics, Nat. Commun. 7 (2016) 10623, https://doi.org/10.1038/ncomms10623.
[8] E. Eroglu, S. Hallström, H. Bischof, M. Opelt, K. Schmidt, B. Mayer, M. Waldeck-Weiermair, W.F. Graier, R. Malli, Real-time visualization of distinct nitric oxide generation of nitric oxide synthase isoforms in single cells, Nitric Oxide 70 (2017) 59–67, https://doi.org/10.1016/j.niox.2017.09.001.
[9] H. Li, Z. Cheng, H. Li, Y. Yin, Y. Li, T. Chen, X. Dong, Q. Hu, D. Wu, A novel genetically encoded indicator for deciphering cytosolic and mitochondrial nitric oxide in live cells, Biochem. Biophys. Res. Commun. 749 (2025) 151345, https://doi.org/10.1016/j.bbrc.2025.151345.
[10] O.M. Subach, P.J. Cranfill, M.W. Davidson, V.V. Verkhusha, An enhanced monomeric blue fluorescent protein with the high chemical stability of the chromophore, PloS One 6 (2011) e28674, https://doi.org/10.1371/journal.pone.0028674.
[11] C. Montali, S. Abbruzzetti, A. Franzen, G. Casini, S. Bruno, P. Delcanale, S. Burgstaller, J. Ramadani-Muja, R. Malli, T. Gensch, C. Viappiani, Nitric oxide sensing by a blue fluorescent protein, Antioxidants 11 (2022) 2229, https://doi.org/10.3390/antiox11112229.
[12] L. Cupellini, M. Corbella, B. Mennucci, C. Curutchet, Electronic energy transfer in biomacromolecules, WIREs Comput. Mol. Sci. 9 (2019) e1392, https://doi.org/10.1002/wcms.1392.
[13] R. Olekhnovitch, B. Ryffel, A.J. Müller, P. Bousso, Collective nitric oxide production provides tissue-wide immunity during Leishmania infection, J. Clin. Invest. 124 (2014) 1711–1722, https://doi.org/10.1172/JCI72058.
[14] K. Chen, R.N. Pittman, A.S. Popel, Nitric oxide in the vasculature: where does it come from and where does it go? A quantitative perspective, Antioxid. Redox Signal. 10 (2008) 1185–1198, https://doi.org/10.1089/ars.2007.1959.
[15] C.N. Hall, J. Garthwaite, What is the real physiological NO concentration in vivo? Nitric Oxide 21 (2009) 92–103, https://doi.org/10.1016/j.niox.2009.07.002.
[16] A.P. Gobert, P. Vincendeau, D. Mossalayi, B. Veyret, Mechanism of extracellular thiol nitrosylation by N2O3 produced by activated macrophages, Nitric Oxide 3 (1999) 467–472, https://doi.org/10.1006/niox.1999.0260.
[17] F. Marchesani, E. Gianquinto, I. Autiero, A. Michielon, B. Campanini, S. Faggiano, S. Bettati, A. Mozzarelli, F. Spyrakis, S. Bruno, The allosteric interplay between S-nitrosylation and glycine binding controls the activity of human serine racemase, FEBS J. 288 (2021) 3034–3054, https://doi.org/10.1111/febs.15645.
[18] V. Fernando, X. Zheng, Y. Walia, V. Sharma, J. Letson, S. Furuta, S-nitrosylation: an emerging paradigm of redox signaling, Antioxidants 8 (2019) 404, https://doi.org/10.3390/antiox8090404.
[19] A.J. Sporer, L.J. Kahl, A. Price-Whelan, L.E. Dietrich, Redox-based regulation of bacterial development and behavior, Annu. Rev. Biochem. 86 (2017) 777–797, https://doi.org/10.1146/annurev-biochem-061516-044453.

[20] I.S. Arts, A. Gennaris, J.-F. Collet, Reducing systems protecting the bacterial cell envelope from oxidative damage, FEBS Lett. 589 (2015) 1559–1568, https://doi.org/10.1016/j.febslet.2015.04.057.
[21] J.R. Lackowicz, Principle of Fluorescence Spectroscopy, Kluwer Academic, New York, 1999.
[22] Th. Förster, Intermolecular energy transference and fluorescence, Ann. Phys. 2 (1948) 55–75, https://doi.org/10.1039/F29736900126.
[23] S.E. Braslavsky, E. Fron, H.B. Rodríguez, E.S. Román, G.D. Scholes, G. Schweitzer, B. Valeur, J. Wirz, Pitfalls and limitations in the practical use of Förster's theory of resonance energy transfer, Photochem. Photobiol. Sci. 7 (2008) 1444–1448, https://doi.org/10.1039/b810620g.
[24] R.S. Knox, H. Van Amerongen, Refractive index dependence of the Förster resonance excitation transfer rate, J. Phys. Chem. B 106 (2002) 5289–5293, https://doi.org/10.1021/jp013927+.
[25] M.R. Talipov, Q.K. Timerghazin, Protein control of *S* -nitrosothiol reactivity: interplay of antagonistic resonance structures, J. Phys. Chem. B 117 (2013) 1827–1837, https://doi.org/10.1021/jp310664z.
[26] R.P. Mueller, J.R. Huber, Two rotational isomers of methyl thionitrite: light-induced, reversible isomerization in an argon matrix, J. Phys. Chem. 88 (1984) 1605–1608, https://doi.org/10.1021/j150652a033.
[27] M.D. Bartberger, K.N. Houk, S.C. Powell, J.D. Mannion, K.Y. Lo, J.S. Stamler, E. J. Toone, Theory, spectroscopy, and crystallographic analysis of *S* -nitrosothiols: conformational distribution dictates spectroscopic behavior, J. Am. Chem. Soc. 122 (2000) 5889–5890, https://doi.org/10.1021/ja994476y.
[28] B. Meyer, A. Genoni, A. Boudier, P. Leroy, M.F. Ruiz-Lopez, Structure and stability studies of pharmacologically relevant *S* -nitrosothiols: a theoretical approach, J. Phys. Chem. A 120 (2016) 4191–4200, https://doi.org/10.1021/acs.jpca.6b02230.
[29] C. Ruano, J.C. Otero, J.F. Arenas, J. Soto, Multiconfigurational second-order perturbation study of the photochemical decomposition of methyl thionitrite, Chem. Phys. Lett. 553 (2012) 17–20, https://doi.org/10.1016/j.cplett.2012.09.060.
[30] S. Manna, S. Sinha Ray, P. Ghosh, S. Chattopadhyay, Structural properties and isomerisation of simple S-nitrosothiols: *ab initio* studies with a simplified treatment of correlation effects, Mol. Phys. 118 (2020) e1641639, https://doi.org/10.1080/00268976.2019.1641639.
[31] E. Cignoni, L. Cupellini, B. Mennucci, A fast method for electronic couplings in embedded multichromophoric systems, J. Phys. Condens. Matter 34 (2022) 304004, https://doi.org/10.1088/1361-648X/ac6f3c.
[32] D. Gonzalo, L. Cupellini, C. Curutchet, On the breakdown of Förster energy transfer theory due to solvent effects: atomistic simulations unveil distance-dependent dielectric screening in calmodulin, Chem. Sci. 16 (2025) 3693–3704, https://doi.org/10.1039/d4sc07679f.
[33] S. Han, Force field parameters for S -nitrosocysteine and molecular dynamics simulations of *S* -nitrosated thioredoxin, Biochem. Biophys. Res. Commun. 377 (2008) 612–616, https://doi.org/10.1016/j.bbrc.2008.10.017.
[34] H. Niki, P.D. Maker, C.M. Savage, L.P. Breitenbach, Spectroscopic and photochemical properties of methyl thionitrite (CH3SNO), J. Phys. Chem. 87 (1983) 7–9, https://doi.org/10.1021/j100224a003.
[35] D.L.H. Williams, The chemistry of S-nitrosothiols, Acc. Chem. Res. 32 (1999) 869–876, https://doi.org/10.1021/ar9800439.
[36] P.D. Wood, B. Mutus, R.W. Redmond, The mechanism of photochemical release of nitric oxide from S-nitrosoglutathione, Photochem. Photobiol. 64 (1996) 518–524, https://doi.org/10.1111/j.1751-1097.1996.tb03099.x.
[37] M. Wang, Y. Da, Y. Tian, Fluorescent proteins and genetically encoded biosensors, Chem. Soc. Rev. 52 (2023) 1189–1214, https://doi.org/10.1039/D2CS00419D.
[38] A.M. Gest, A.Z. Sahan, Y. Zhong, W. Lin, S. Mehta, J. Zhang, Molecular spies in action: genetically encoded fluorescent biosensors light up cellular signals, Chem. Rev. 124 (2024) 12573–12660, https://doi.org/10.1021/acs.chemrev.4c00293.
[39] C.E. Paulsen, K.S. Carroll, Cysteine-mediated redox signaling: chemistry, biology, and tools for discovery, Chem. Rev. 113 (2013) 4633–4679, https://doi.org/10.1021/cr300163e.
[40] J. Zhang, Z. Ye, S. Singh, D.M. Townsend, K.D. Tew, An evolving understanding of the S-glutathionylation cycle in pathways of redox regulation, Free Radic. Biol. Med. 120 (2018) 204–216, https://doi.org/10.1016/j.freeradbiomed.2018.03.038.
[41] H. Vázquez-Meza, M.M. Vilchis-Landeros, M. Vázquez-Carrada, D. Uribe-Ramírez, D. Matuz-Mares, Cellular compartmentalization, glutathione transport and its relevance in some pathologies, Antioxidants 12 (2023) 834, https://doi.org/10.3390/antiox12040834.